catalysts

IMPACT FACTOR 3.9

CITESCORE 6.3

Article

Density Functional Theory Study of CuAg Bimetal Electrocatalyst for CO_2RR to Produce CH_3OH

Sensen Xue, Xingyou Liang, Qing Zhang, Xuefeng Ren, Liguo Gao, Tingli Ma and Anmin Liu

Special Issue

Theoretical and Computational Studies of Catalytic Reactions

Edited by

Dr. Anmin Liu and Dr. Xuefeng Ren

MDPI

https://doi.org/10.3390/catal14010007

catalysts

MDPI

Article

Density Functional Theory Study of CuAg Bimetal Electrocatalyst for CO_2RR to Produce CH_3OH

Sensen Xue [1], Xingyou Liang [1], Qing Zhang [1], Xuefeng Ren [2], Liguo Gao [1], Tingli Ma [3,4] and Anmin Liu [1,*]

[1] State Key Laboratory of Fine Chemicals, School of Chemical Engineering, Dalian University of Technology, Dalian 116081, China; xuess@mail.dlut.edu.cn (S.X.)
[2] School of Ocean Science and Technology, Dalian University of Technology, Panjin 124221, China
[3] Department of Materials Science and Engineering, China Jiliang University, Hangzhou 310018, China; tinglima@life.kyutech.ac.jp
[4] Graduate School of Life Science and Systems Engineering, Kyushu Institute of Technology, 2-4 Hibikino, Wakamatsu, Kitakyushu 808-0196, Fukuoka, Japan
* Correspondence: liuanmin@dlut.edu.cn

Abstract: Converting superfluous CO_2 into value-added chemicals is regarded as a practical approach for alleviating the global warming problem. Powered by renewable electricity, CO_2 reduction reactions (CO_2RR) have attracted intense interest owing to their favorable efficiency. Metal catalysts exhibit high catalytic efficiency for CO_2 reduction. However, the reaction mechanisms have yet to be investigated. In this study, CO_2RR to CH_3OH catalyzed by CuAg bimetal is theoretically investigated. The configurations and stability of the catalysts and the reaction pathway are studied. The results unveil the mechanisms of the catalysis process and prove the feasibility of CuAg clusters as efficient CO_2RR catalysts, serving as guidance for further experimental exploration. This study provides guidance and a reference for future work in the design of mixed-metal catalysts with high CO_2RR performance.

Keywords: CuAg bimetal; CO_2RR; pathway; theoretical study

Citation: Xue, S.; Liang, X.; Zhang, Q.; Ren, X.; Gao, L.; Ma, T.; Liu, A. Density Functional Theory Study of CuAg Bimetal Electrocatalyst for CO_2RR to Produce CH_3OH. *Catalysts* **2024**, *14*, 7. https://doi.org/10.3390/catal14010007

Academic Editor: Igor A. Pašti

Received: 11 November 2023
Revised: 11 December 2023
Accepted: 18 December 2023
Published: 20 December 2023

1. Introduction

The increasing emissions of greenhouse gases such as CO_2 and CH_4 into the air fuels the greenhouse effect and the concomitant global warming. The increase of the concentration of CO_2 has the greatest impact on rising global temperatures. Owing to its important environmental and economic repercussions, reducing carbon emissions without affecting social and economic development has become one of the most urgent problems in China.

Before now, numerous strategies have been developed to reduce the concentration of CO_2 in the atmosphere, such as CO_2 capture and storage [1], absorption [2], and chemical conversion [3–6]. In recent years, the conversion of CO_2 into a variety of economically valuable chemicals has emerged as a promising technology [7,8]. In this regard, electrochemical CO_2 reduction (CO_2RR) stands out because of its high value-added products (including ethanol and methanol) and its favorable conversion efficiency [9–13]. Among the various catalysts for CO_2RR, copper (Cu) is widely used because of its abundance and ambient-environment working conditions; however, its limited activity and selectivity has hindered further development [14–18]. Consequently, recent research efforts have been devoted to enhancing its catalytic performance by adjusting catalyst properties such as particle size [19], shape [20–22], and grain boundary [23].

As a result, more attractive Cu-based bimetallic CO_2RR catalysts with enhanced activity and selectivity have been discovered [24–28]. Thus, Kim et al. [29] reported a CuAu catalyst demonstrating high CO selectivity (~80%) in an overpotential of ~200 mV. Zhang et al. [30] fabricated a CuPd nanoalloy with a twofold enhancement in Faradaic efficiency for CO_2RR to methane compared with Cu alone. Sarfraz et al. [31] reported a stable CuSn catalyst exhibiting a Faradaic efficiency for CO_2RR to CO greater than 90%

and a current density of -1.0 mA cm^{-2} at -0.6 V vs. a reversible hydrogen electrode (RHE). Chungseok et al. [32] reported on the performance of a CuAg nanowire. The Cu-Ag interface of the CuAg nanowire significantly improved the selectivity of CO_2 reduction to CH_4, with a maximum Faraday efficiency (FE) of 72% production at -1.17 V (relative to an RHE). Nevertheless, studies on Cu bimetallic catalysts inducing CO_2RR to alcohol are scarce, and a more fundamental understanding is required for the rational design of Cu-based catalysts in this field.

After much research, significant progress has been made in CO_2RR, especially in experimental studies. However, traditional experimental methods have inherent limitations, including blindness, workload, time, and resource waste. Nowadays, quantum chemistry and molecular dynamic simulations are widely used for calculating and simulating chemical systems as a technique to understand and predict behaviors at the molecular level [33–37]. Combining computational chemistry predictions with experimental investigation is a highly efficient methodology for accelerating the investigation of CO_2RR. In electrocatalysis research, the density functional theory (DFT) is widely used to analyze possible reaction path energy changes, reaction mechanisms, and catalyst materials for special reactions, such as CO_2RR, NRR, ORR, and so on [38]. CH_3OH is one of the most important chemicals used as a green fuel or the intermediate of reactions. It can be directly used in energy conversion systems such as methanol fuel cells or internal combustion engines, due to its relatively high energy density.

In this study, we theoretically designed a series of CuAg bimetallic clusters and investigated their feasibility as catalysts for CO_2RR to methanol according to the DFT. Considering that Ag nanoparticles have been previously shown to act as nucleation seeds for CuAg particles [39], we selected the most stable Ag cluster as a basis for the design of CuAg clusters with different configurations. Then, the CO_2 adsorption behavior on different sites was evaluated. Finally, the reaction pathway was fully studied to determine the optimal CuAg cluster configuration. This work sought to experimentally study a series of CuAg bimetallic cluster catalysts and establish a screening mechanism to calculate the catalytic activity of reducing CO_2RR to CH_3OH. This work can serve as guidance for further experimental exploration.

2. Results and Discussion

2.1. Study on the Stability of the Ag Clusters

In contrast with Ag_1 and Ag_2 clusters, which exhibit only one structure, different isomers appear when the number of Ag atoms (n) is $n \geq 3$. In this case, the most stable configuration among these isomers must be screened. For n = 3, there are two isomers, i.e., linear and triangular, with similar bond lengths according to the calculation. By comparing their total energy and binding energy (Table S1), it was found that the binding energy of the triangular isomer is lower than that of its linear counterpart. Therefore, the most stable structure of the Ag_3 cluster is a flat regular triangle; its optimized structure is shown in Figure S1.

When n = 4, Ag_4 exhibits five isomeric structures (Figure S2), among which the most stable is a flat rhombus. For n = 5, the most stable configuration is a plane isosceles trapezoid composed of three triangles. Moreover, when n = 6, a two-dimensional close-packed shape composed of four triangles has the lowest binding energy and is therefore the most stable. Surprisingly, these selected structures are all planar (the corresponding calculation results can be found in Supplementary Information).

Figure 1 depicts the most stable Ag_n cluster structures for n = 1–6. The relationship between the stability of the six clusters and the number of Ag atoms is analyzed in Figure 2. As can be seen, the binding energy (E_B) has a downward trend, indicating that the total energy required for cluster binding decreases as the number of atoms increases. However, since the number of Ag atoms differs between clusters, the overall E_B cannot be used to compare their stability, and the average binding energy (E_b) needs to be introduced. The calculated values of E_b are shown in Table S5. It was found that E_b decreases with the

increase of n, reaching the smallest value (indicative of the highest cluster stability) for n = 6. Therefore, the Ag_6 clusters were selected for the following experiments.

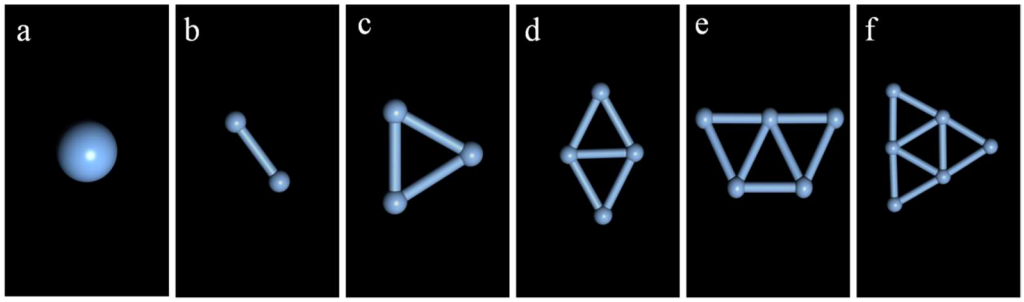

Figure 1. Most stable configurations of Ag_n (n = 1–6) clusters: (**a**) Ag_1; (**b**) Ag_2; (**c**) Ag_3; (**d**) Ag_4; (**e**) Ag_5; (**f**) Ag_6.

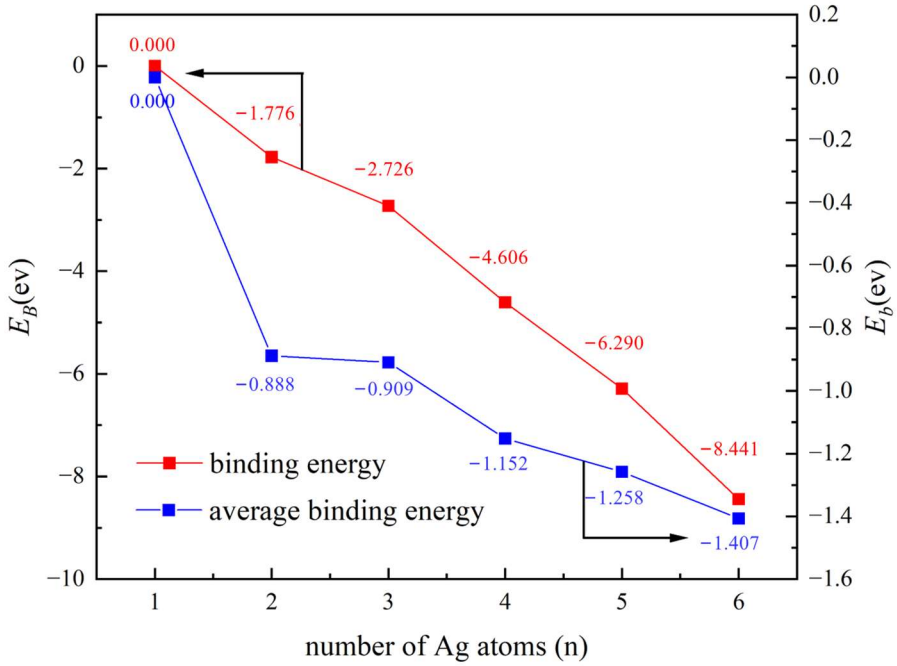

Figure 2. Variation of binding energy and average binding energy with the number of Ag atoms.

2.2. Study on the Stability of the CuAg Clusters

The selected Ag_6 clusters were doped with Cu atoms, and the changes in parameters such as bond length, bond angle, and stability after doping were examined. When doped with a Cu atom, the resulting Cu_1Ag_5 cluster has two kinds of isomers. The specific structures are shown in Figure 3. Although the two structures have symmetry, the addition of Cu changes the structure of the Ag cluster, which loses its regular triangle structure. Calculation of the total energy and average binding energy of the two structures (Table S6) revealed that structure *a* is relatively stable in comparison to structure *b*. According to the method mentioned above, the most stable configurations of the $Cu_{6-n}Ag_n$ (n = 1–5) clusters shown in Figure 4 were obtained.

The HOMO and LUMO values of the six structures in Figure 4 were simulated and calculated. Figure 5 shows that the E_{LUMO} decreases after doping with Cu, indicating that the presence of the Cu atoms enhances the electron-accepting ability of the Ag clusters. Moreover, the E_{HOMO} of the bimetallic clusters decreases after Cu doping, indicating that the addition of Cu atoms reduces the electron-donating ability. The ΔE value is not significantly changed by Cu doping, and the ΔE of Cu_5Ag_1 is the smallest, which suggests that the electron transfer is the fastest in this cluster.

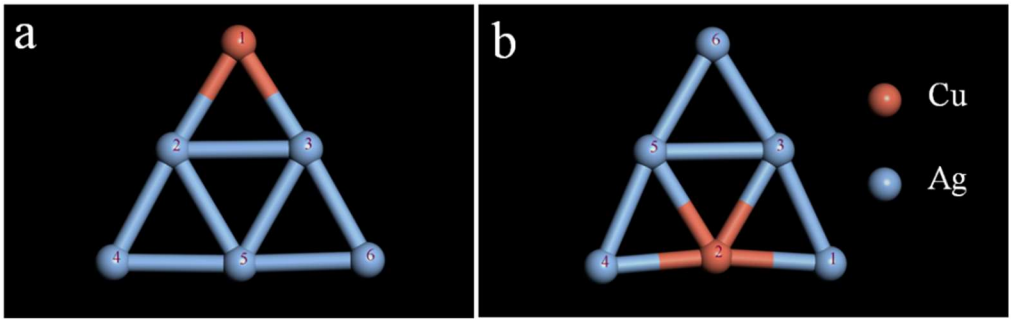

Figure 3. Isomeric structure of Cu_1Ag_5 clusters: (**a**) Cu is the tip position; (**b**) Cu is the middle position.

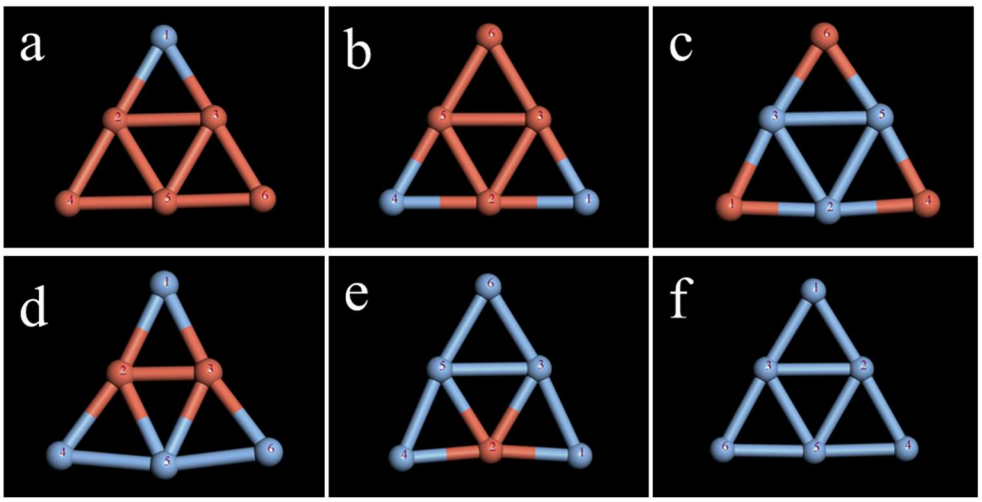

Figure 4. Most stable configuration of $Cu_{6-n}Ag_n$ (n = 1–6) clusters: (**a**) Cu_5Ag_1; (**b**) Cu_4Ag_2; (**c**) Cu_3Ag_3; (**d**) Cu_2Ag_4; (**e**) Cu_1Ag_5; (**f**) Ag_6.

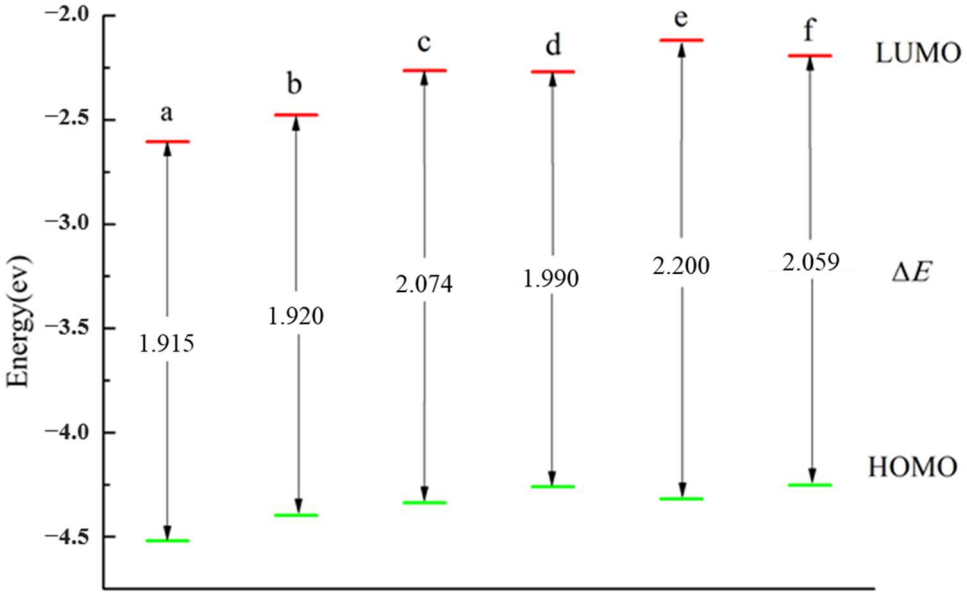

Figure 5. Frontier molecular orbital energy level and ΔE of the $Cu_{6-n}Ag_n$ cluster: (**a**) Cu_5Ag_1, (**b**) Cu_4Ag_2, (**c**) Cu_3Ag_3, (**d**) Cu_2Ag_4, (**e**) Cu_1Ag_5, and (**f**) Ag_6.

2.3. Study on the CO_2 Adsorption Stability of the CuAg Clusters

Table 1 lists the values of the first four atoms with the largest absolute Fukui index of the six cluster structures. Because some clusters have symmetry, the Fukui indices of atoms

that are structurally axisymmetric are equal. CO_2 is easily adsorbed on atoms with small Fukui (-) values because the structure is stable after adsorption; therefore, cluster catalysts with small Fukui indices would exhibit enhanced CO_2 activation.

Table 1. Fukui indices of CuAg clusters.

Configuration	Site	Value	Site	Value	Site	Value	Site	Value
a	Cu (4/6)	+0.237	Ag (1)	−0.228	Cu (4/6)	−0.204	Ag (1)	+0.175
b	Cu (6)	+0.276	Ag (1/4)	−0.229	Cu (6)	−0.185	Ag (1/4)	+0.183
c	Ag (1)	+0.233	Ag (4/6)	+0.221	Ag (1)	−0.219	Ag (4/6)	−0.217
d	Ag (1)	+0.238	Ag (4/6)	−0.252	Ag (4/6)	+0.211	Ag (1)	−0.182
e	Ag (1/4)	−0.252	Ag (6)	+0.241	Ag (1/4)	+0.210	Ag (6)	−0.206
f	Ag (1/4/6)	−0.234	Ag (1/4/6)	−0.231	Ag (2/3/5)	+0.103	Ag (2/3/5)	−0.102

CO_2 adsorption proceeds mainly by two processes, i.e., single-site adsorption and dual-site adsorption. For the Cu_5Ag_1 cluster, the absolute Fukui value (−) of the silver atom at position 1 is the largest, and CO_2 adsorption is therefore preferred at this site. The specific stable structure after adsorption is shown in Figure 6, and the bond lengths, bond angles, and energies of the Cu_5Ag_1–CO_2 structure are summarized in Table 2. In double-site adsorption, comparison of the C–O bond length before and after adsorption reveals that two C–O bonds of CO_2 elongate and the third shortens in structures *a* and *c*. In contrast, the two bond lengths of CO_2 in structure *b* remain virtually unaltered after adsorption. These results suggest that structures *a* and *c* are more conducive to inducing CO_2 reduction to alcohols. Then, by comparing the adsorption energy of structures *a* and *c*, it can be concluded that structure *a* is the best for double-site adsorption of CO_2.

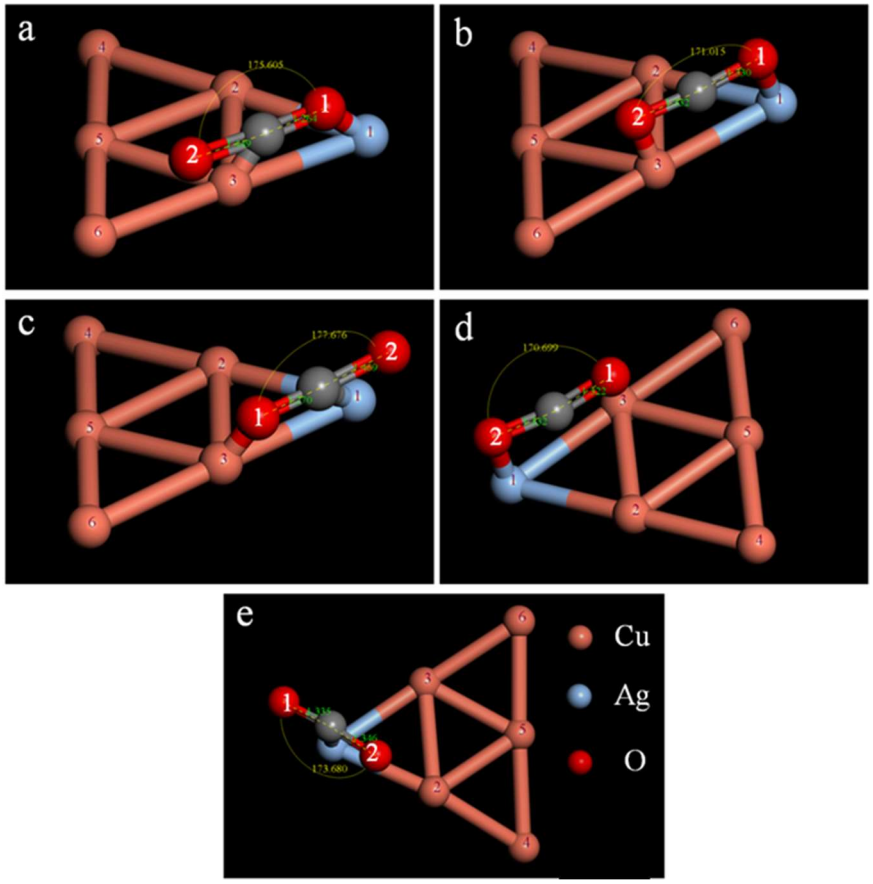

Figure 6. Isomers of the Cu_5Ag_1–CO_2 adsorption structure (**a**–**c**) are dual-site adsorption, while (**d**,**e**) are single-site adsorption.

Table 2. Bond lengths, bond angles, and energies of the Cu_5Ag_1–CO_2 structures.

Isomers	∠O1CO2/°	d_{C-O1}/Å	d_{C-O2}/Å	$E_{CuAg-CO2}$/Ha	E_{obs}/eV
a	175.605	1.264	1.449	−13,589.920	−0.555
b	171.015	1.330	1.332	−13,589.911	−0.299
c	177.676	1.270	1.469	−13,589.905	−0.1439
d	170.699	1.322	1.332	−13,589.911	−0.301
e	173.680	1.335	1.346	−13,589.906	−0.163

For single-site adsorption, the CO_2 bond length in structure *d* does not change significantly, whereas the change in structure *e* is more obvious, indicating a higher probability of CO_2 activation when C atoms are adsorbed on Cu_5Ag_1.

Similarly, the best adsorption configurations for double-site adsorption and single-site adsorption were obtained for the other clusters, as shown in Figures 7 and 8. The calculation results show that the adsorption method, the CO_2 activation degree, and the overall stability after adsorption are different between clusters.

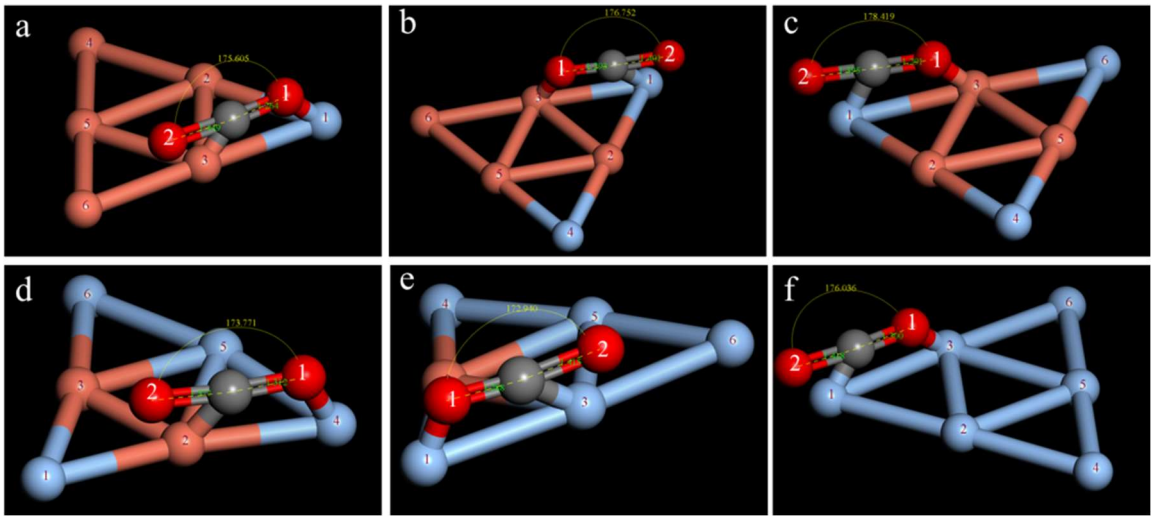

Figure 7. Optimal CO_2 adsorption structure in the Cu_nAg_{6-n} cluster (n = 1–6) for dual-site adsorption: (**a**) Cu_5Ag_1; (**b**) Cu_4Ag_2; (**c**) Cu_3Ag_3; (**d**) Cu_2Ag_4; (**e**) Cu_1Ag_5; (**f**) Ag_6.

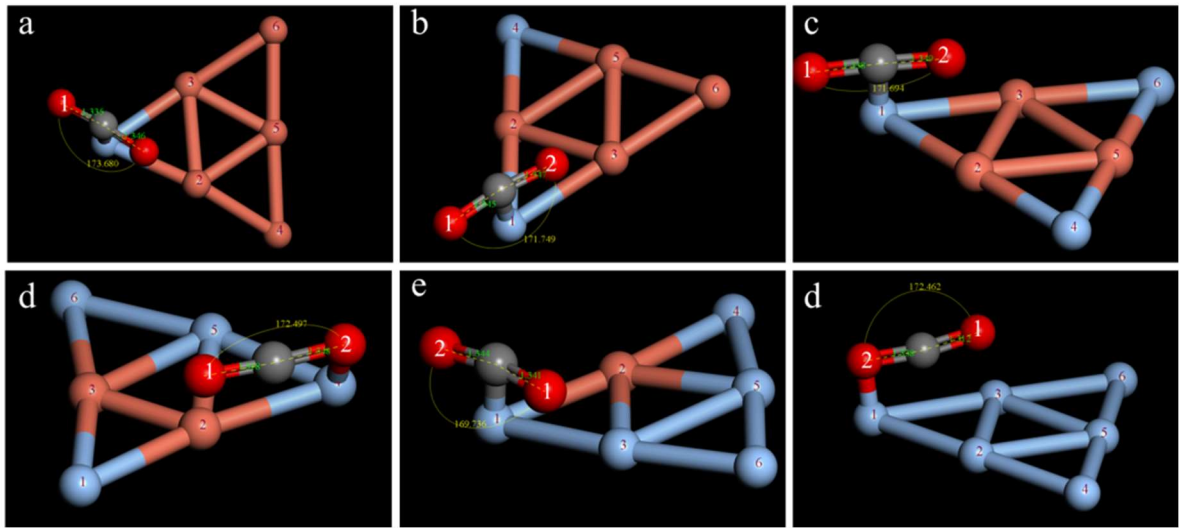

Figure 8. Optimal CO_2 adsorption structure in the Cu_nAg_{6-n} cluster (n = 1–6) for single-site adsorption: (**a**) Cu_5Ag_1; (**b**) Cu_4Ag_2; (**c**) Cu_3Ag_3; (**d**) Cu_2Ag_4; (**e**) Cu_1Ag_5; (**f**) Ag_6.

2.4. Pathway Study on CO_2RR to CH_3OH

The mechanism of the CO_2 reduction reaction is still unclear, and further experimental and theoretical research is needed. Recently, the reaction pathway of CO_2 hydrogenation reduction to CH_3OH has been studied [40,41]. Figure 9 depicts the preferred reaction mechanism of CO_2 hydrogenation to obtain CH_3OH; thus, this route was selected to study the catalytic effect of the CuAg clusters. The specific reaction intermediates are CO_2*, HCOO*, HCOOH*, H_2COOH*, TS4, CH_2O*, TS5, CH_3O*, and CH_3OH.

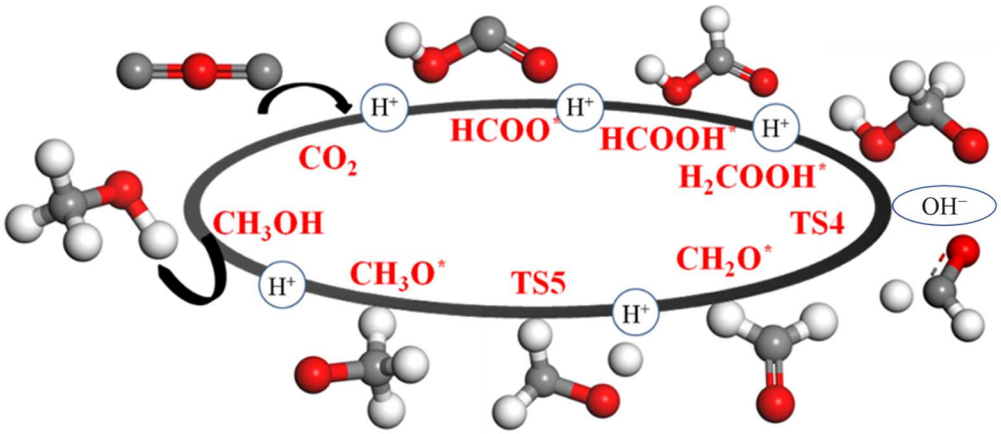

Figure 9. Reaction pathway of CO_2 hydrogenation to CH_3OH.

The Gibbs free energy (ΔG) of the reactions involving intermediates, reactants, and products was calculated at 298.15 K, using the CO_2 reactant as a benchmark. The results are shown in Table S16. Similarly, the adsorption structures of all products, intermediates, reactants, and catalysts were simulated according to the previous calculation structure. Structure optimization and ΔG calculation were performed using the same method.

The calculated energy values of the Cu_5Ag_1 cluster are listed in Table S17, and the corresponding ladder diagram is shown in Figure 10. It can be seen that in the absence of a catalyst, the ΔG of the intermediates gradually rises, and the energy difference between CO_2 and CH_3OH is 389.422 eV, which indicates that the reaction is not spontaneous under normal conditions.

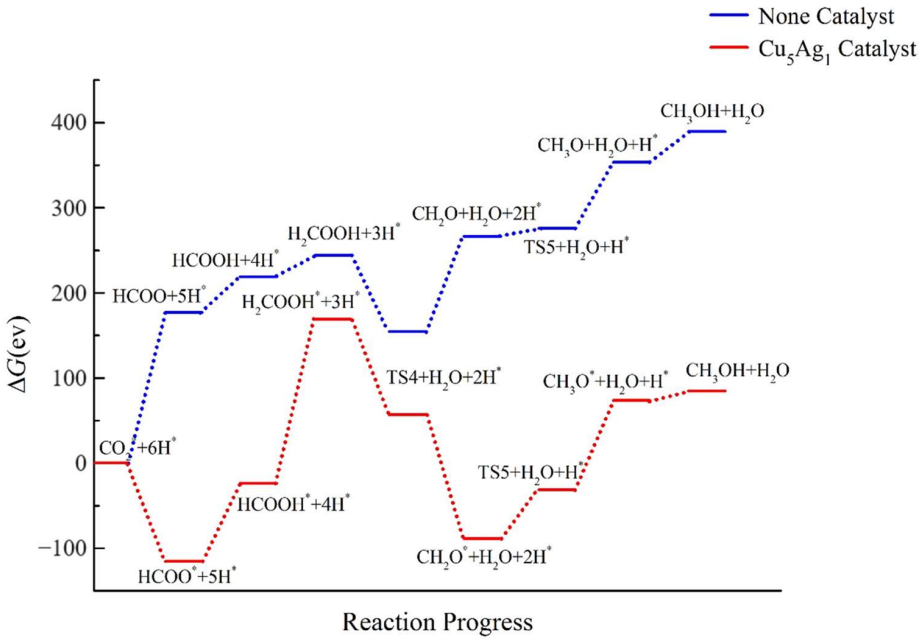

Figure 10. Energy diagram of CO_2 hydrogenation to CH_3OH catalyzed by the Cu_5Ag_1 cluster.

When the Cu_5Ag_1 catalyst is added, the ΔG of the intermediate decreases compared with that obtained without the catalyst, indicating that the cluster has a certain degree of catalytic activity for the CO_2 reduction reaction. After adding the Cu_5Ag_1 cluster, the difference between the energy of the CH_3OH product and that of CO_2 is only 84.709 eV. Compared with the results without a catalyst, although ΔG is reduced by about four times, it is still positive, indicating that the reaction cannot proceed spontaneously in the presence of Cu_5Ag_1. Therefore, it can be concluded that the Cu_5Ag_1 cluster has a catalytic effect on the reaction, albeit a small one.

The energy ladder diagram of the Cu_4Ag_2 cluster reduction is shown in Figure 11. Certain catalytic activity on CO_2RR was detected for the Cu_4Ag_2 cluster by comparing the ΔG of each intermediate and the blank control data. Specifically, the catalyst decreases the ΔG of each intermediate, this decrease being the largest in HCOO* and TS4. In the absence of a catalyst, CO_2 has the lowest ΔG in all the pathways, but this trend changes after adding Cu_4Ag_2. For the CH_3OH product, after adding the Cu_4Ag_2 catalyst, ΔG decreases by 259.869 eV. Therefore, the Cu_4Ag_2 catalyst can induce the formation of CH_3OH to some extent, reducing the reaction energy barrier and softening the reaction conditions. However, the ΔG of CH_3OH is still positive, indicating that the catalytic effect of the cluster is not ideal.

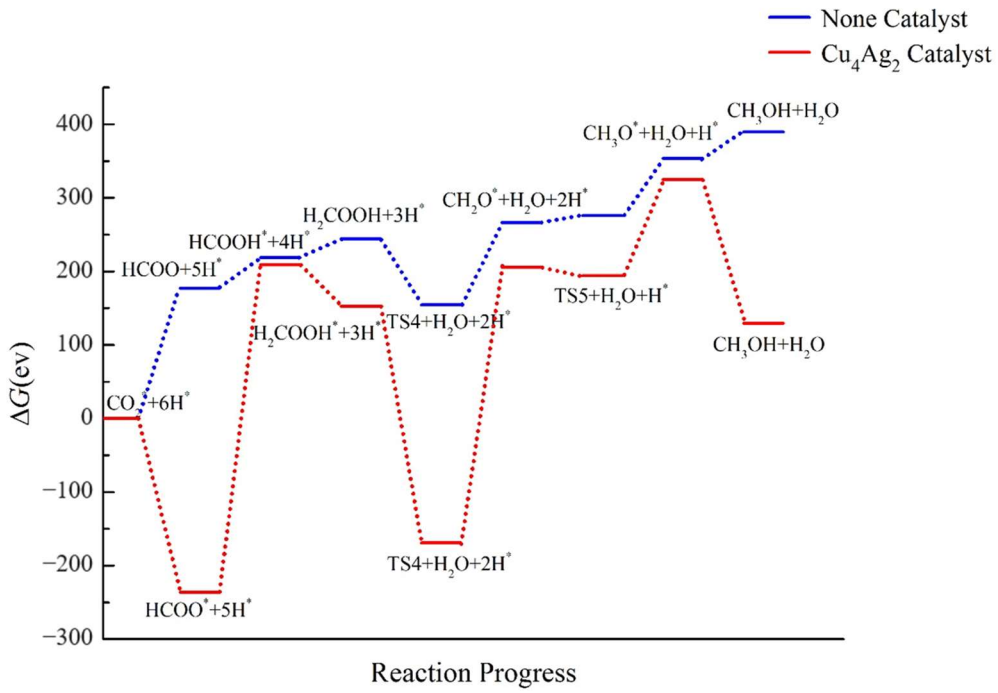

Figure 11. Energy diagram of CO_2 hydrogenation to CH_3OH catalyzed by the Cu_4Ag_2 cluster.

The calculation results of the Cu_3Ag_3 cluster are shown in Figure 12. It was found that after the addition of the Cu_3Ag_3 cluster catalyst, the ΔG of the CO_2 hydrogenation route undergoes a major change. In the absence of a catalyst, the energy of the intermediates gradually rises, whereas this trend is reversed after adding the Cu_3Ag_3 catalyst. The catalyst reduces the ΔG of most of the intermediates in the entire path, among which HCOO*, H_2COOH*, and CH_3O* exhibit the largest decrease, indicating that the catalyst can promote the formation of the three intermediates. However, the ΔG of the transition state TS4 is higher by about 23 eV than that obtained without catalysis, which suggests that the bimetallic Cu_3Ag_3 cluster could not promote the formation of TS4. For the CH_3OH product, after adding the Cu_3Ag_3 cluster catalyst, the ΔG of CH_3OH decreases by 152.792 eV, indicating that the catalyst can effectively reduce the energy barrier of the reaction path. However, since the ΔG of the intermediate product increases, the catalytic effect of the Cu_3Ag_3 cluster on CO_2RR is not significant either.

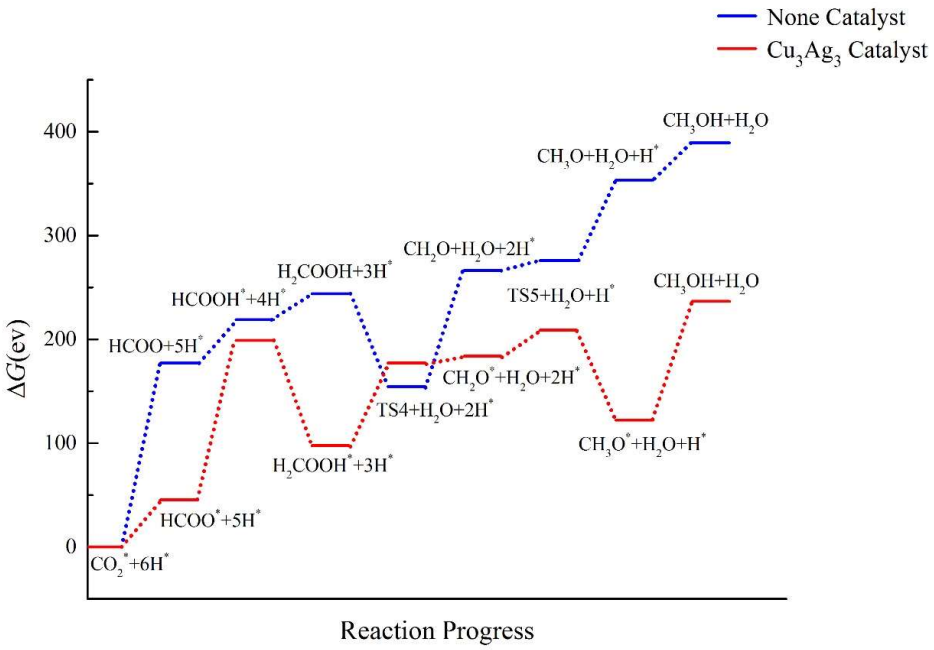

Figure 12. Energy diagram of CO_2 hydrogenation to CH_3OH catalyzed by the Cu_3Ag_3 cluster.

Figure 13 shows the energy ladder diagram of CO_2RR to CH_3OH after adding the bimetallic Cu_2Ag_4 cluster catalyst. The ΔG of all intermediates and products decreases significantly. Compared with the results of the reaction without a catalyst, the ΔG values of all intermediates and reactants decrease directly from positive to negative, indicating that the hydrogenation of CO_2 to CH_3OH can occur spontaneously in the presence of the Cu_2Ag_4 catalyst. Therefore, the Cu_2Ag_4 cluster displays sufficient catalytic activity on the CO_2RR to CH_3OH.

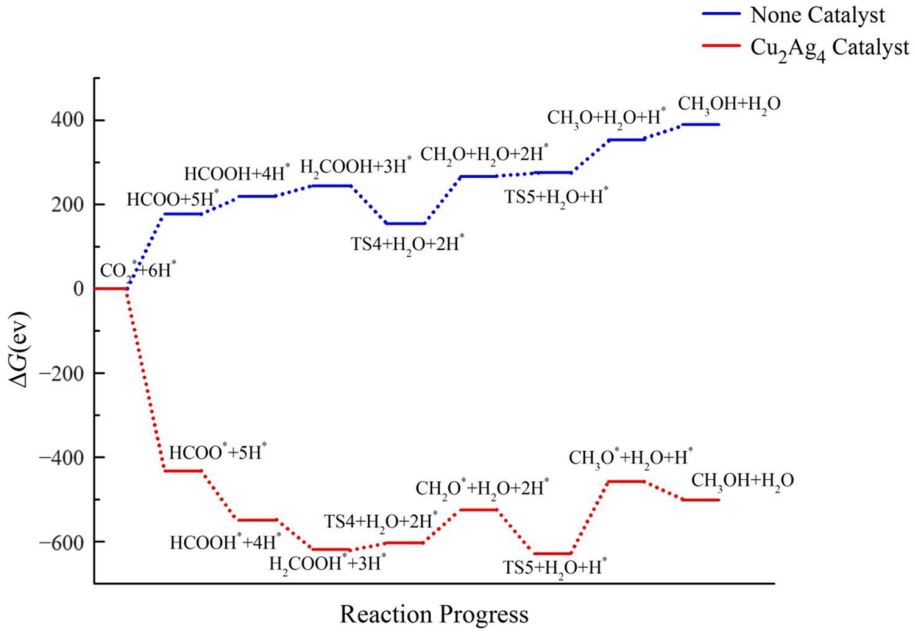

Figure 13. Energy diagram of CO_2 hydrogenation to CH_3OH catalyzed by the Cu_2Ag_4 cluster.

The catalytic effect of the cluster doped with one Cu atom is shown in Figure 14. From the overall diagram, it can be deduced that the cluster has a good catalytic effect, because the ΔG of the six intermediates is lower than that of CO_2. However, the ΔG of the TS5 intermediate is higher than that of CO_2, and the ΔG of TS5 is positive. Focusing on the

CH_3OH product, it can be seen that the ΔG of CH_3OH after the addition of the catalyst does not differ much from that of CO_2; the difference is only 23.456 eV. This indicates that the reaction is more favorable after adding Cu_1Ag_5. Therefore, the Cu_1Ag_5 cluster can promote the reaction of CO_2 to CH_3OH, but the overall catalytic effect is not as significant as that of Cu_2Ag_4.

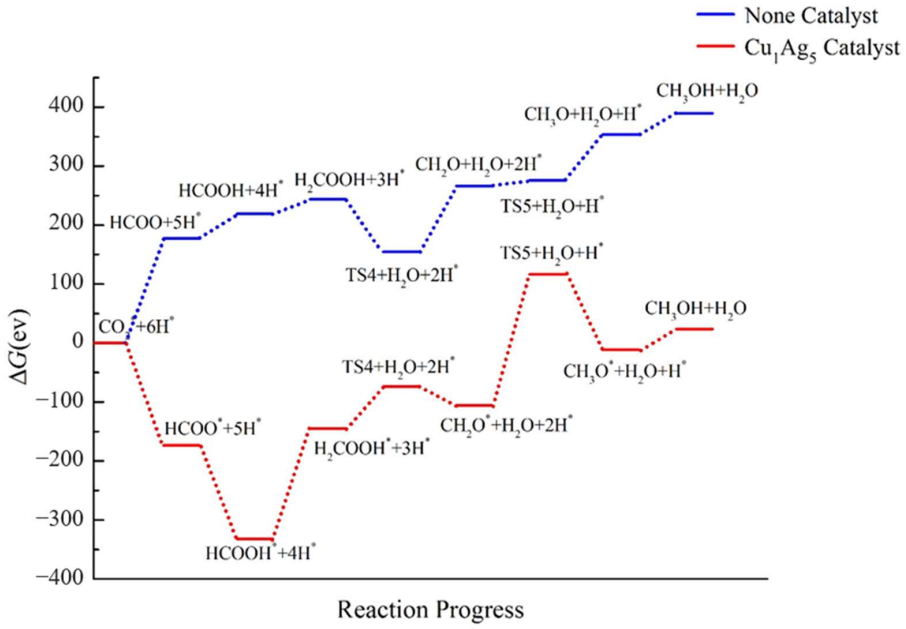

Figure 14. Energy diagram of CO_2 hydrogenation to CH_3OH catalyzed by the Cu_1Ag_5 cluster.

Next, we analyzed the catalytic effect of a pure silver cluster Ag_6. The specific calculation results are shown in Figure 15. The reaction pathway with the Ag_6 cluster is completely different from those of the bimetallic catalysts, and no catalytic effect on CO_2RR is observed. The energy barrier that needs to be overcome after adding the catalyst Ag_6 cluster is higher than the energy barrier present when no catalyst has been added, indicating that the pure metal Ag_6 cluster catalyst would require more severe reaction conditions and would destabilize the intermediates. The Ag_6 cluster cannot promote the formation of the intermediates in the CO_2RR to CH_3OH.

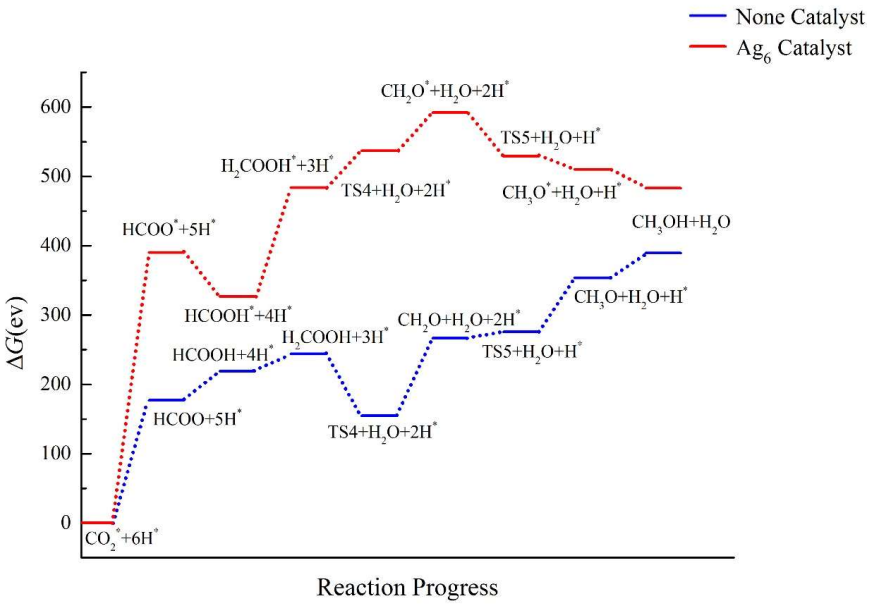

Figure 15. Energy diagram of CO_2 hydrogenation to CH_3OH catalyzed by the Ag_6 cluster.

The energy ladder diagrams of the bimetallic CuAg clusters and the pure metal Ag_6 cluster can be directly compared in Figure 16. It can be seen that the ΔG value of the path is higher for Ag_6 than for the CuAg clusters, indicating that the energy barrier that needs to be overcome for the reaction to proceed is the highest, and the catalytic effect of Ag_6 is the worst. This result demonstrates that Cu doping can indeed increase the catalytic activity of the clusters, which is further confirmed by the experimental results of single-site adsorption of CO_2 (the corresponding data can be found in the supporting information).

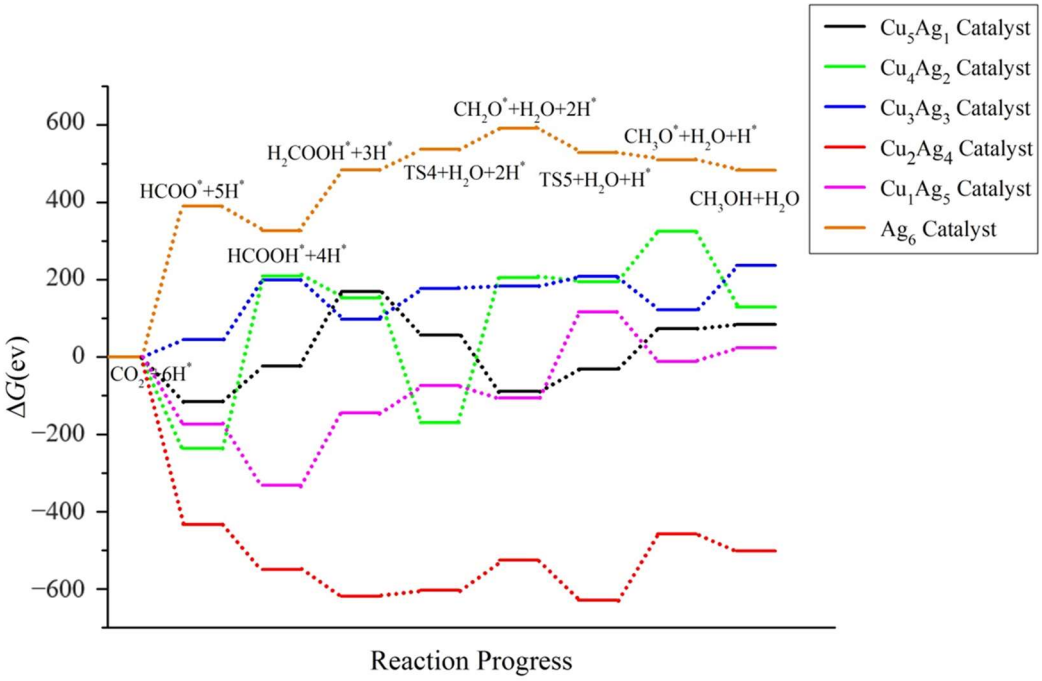

Figure 16. Energy diagram of CO_2 hydrogenation to CH_3OH catalyzed by the CuAg clusters.

By comparing the catalytic activity of the doped bimetallic clusters, it was found that the ΔG of intermediates and the product obtained with Cu_2Ag_4 exhibits the largest decrease among the clusters, and the ΔG of all the intermediates decreases to negative values. This shows that the Cu_2Ag_4 catalyst can significantly improve the stability of the reaction intermediates, thereby facilitating their generation and promoting the spontaneous progress of the reaction. Therefore, among all the catalysts, Cu_2Ag_4 exhibits the best catalytic activity.

3. Models and Methods

This study primarily used the $DMol^3$ module in the Materials Studio software (version 2017), employing spin-polarized DFT to draw the structure, optimize the cluster structure, and calculate the energy. The parameters were set as follows: Functional function selects generalized gradient approximation and Perdew–Burke–Ernzerhof (PBE), the maximum iteration in energy calculation was 1000 times, and "Use symmetry" was selected. In the electronic module, the integration accuracy and self-consistent field (SCF) tolerances were both set to medium. In the basis set, double numerical plus polarization (DNP) was selected, and the basis file was set to 4.4. In the SCF module, the maximum SCF expansion was set to 1000 times, with "Use smearing to tail" checked. In the solvent module, the "Use COSMO solution environment" was set to "water".

Before designing the CuAg bimetallic cluster catalyst, the method by which it will be determined whether the catalyst itself is stable should be clarified. The binding energy *E* is calculated by quantification, and the formula is as follows (1)–(3).

3.1. The Cluster Stability and CO_2 Adsorption Structure Data Analysis

To calculate the binding energy E_B, find the total energy after the final step of convergence is successful in the calculation result file, and bring the total energy into Formula (1). For Ag clusters, the smaller the binding energy is, the more stable the structure is.

$$E_B = E_{Agn} - \mathrm{n} \times E_{Ag} \quad (1)$$

The smaller the average binding energy (E_b) of each atom, the lower the stored energy and the more stable the structure of the whole cluster. The average binding energy of the Ag cluster is found using Formula (2), and that of the CuAg metal cluster is found using Formula (3).

$$E_b = E_{Agn}/\mathrm{n} - E_{Ag} \quad (2)$$

$$E_b = [E_{CuAg} - \mathrm{n} \times E_{Ag} - (6 - \mathrm{n}) \times E_{Cu}]/6 \quad (3)$$

The adsorption energy $E_{CuAg-CO_2}$ is obtained from Formula (4). The smaller the adsorption energy, the more stable the overall structure after adsorption and the greater the change in the C–O bond length, indicating that the catalyst has a better degree of CO_2 activation.

$$E_{ads} = E_{CuAg\text{-}CO_2} - E_{CuAg} - E_{CO_2} \quad (4)$$

3.2. Data Analysis of CO_2 Hydrogenation Reduction Path

At 298.15 K, the Gibbs free energy of reacting all monomers is based on CO_2, and the respective ΔG is obtained. The two sets of ΔG data calculated with and without the catalyst were made into an energy ladder diagram to analyze the catalytic effect of CuAg clusters.

3.3. The HOMO, LUMO and ΔE of the Cluster

The highest occupied molecular orbital (HOMO) and lowest unoccupied molecular orbitals (LUMO) eigenvalues, the HOMO-LUMO gap, and the Fukui function are the most commonly used parameters to estimate the performance of a designed catalyst. The HOMO represents the highest occupied molecular orbital. The higher the E_{HOMO}, the easier it is for CuAg clusters to give electrons. The LUMO represents the lowest unoccupied molecular orbital. The lower the E_{LUMO}, the easier it is for CuAg clusters to obtain electrons. The magnitude of the energy band gap value ($\Delta E = E_{\mathrm{LUMO}} - E_{\mathrm{HOMO}}$) governs the electron transfer rate in the CuAg cluster. The smaller the ΔE, the faster the electron transfer rate between the HOMO and LUMO orbitals.

3.4. Calculation of the Fukui Index of Atoms in the Cluster

The smaller the Fukui (−) value of an atom, the more easily the atom is attacked by a Lewis base; the larger the Fukui (+) of the atom, the more easily the atom is attacked by a Lewis acid. Because CO_2 is a Lewis base, the smaller the Fukui (−) value, the more stable the structure will be after CO_2 adsorption. The better the degree of activation of the cluster catalyst to CO_2, the more easily the atom becomes the best adsorption site for CO_2.

4. Conclusions

On the basis of quantum chemistry theory, the stability of pure Ag metal clusters and bimetallic CuAg clusters and the CO_2 adsorption activity and catalytic effect of the CuAg clusters on the CO_2 hydrogenation to CH_3OH were analyzed by energy calculation and optimization of the constructed structures. The following conclusions were obtained: The most stable configurations of Ag_n (n = 1–6) metal clusters are planar. The stability of the configurations increases with the symmetry. When the adsorption site and adsorption mode of CO_2 on the cluster catalyst are different, the degree of activation of the catalyst and the stability after the adsorption of CO_2 are also different. Doping Cu atoms in the Ag cluster can improve the catalytic activity toward CO_2 hydrogenation to CH_3OH, with the Cu_2Ag_4 cluster

affording the best results. This theoretical study provides guidance and a reference for future work in the design of mixed-metal catalysts with high CO_2RR performance.

Based on theoretical calculations, the relationship between a catalyst's structure, composition, and catalytic CO_2RR activity is constructed, which can be used to guide the preparation of the catalyst and better study the reaction path and mechanism of CO_2RR synthesis of CH_3OH. This has important theoretical and practical significance for promoting research and development of catalytic CO_2RR synthesis of CH_3OH. This article establishes a database for future research and further guides the experimental study of catalysts for reducing CO_2 to CH_3OH. In future studies, theoretical research will be used in the catalytic CO_2RR to produce alcohols, methane, formic acid, and formaldehyde.

Supplementary Materials: The following supporting information can be downloaded at: https://www.mdpi.com/article/10.3390/catal14010007/s1.

Author Contributions: Investigation, S.X., X.L. and Q.Z.; writing—original draft preparation, S.X., X.L., Q.Z. and A.L.; writing—review and editing, X.R., L.G. and T.M. All authors have read and agreed to the published version of the manuscript.

Funding: The support of the Fundamental Research Funds for the Central Universities (DUT22LK09), the Open Foundation of Key Laboratory of Industrial Ecology and Environmental Engineering, MOE (KLIEEE-20-01, KLIEEE-21-02), the Foundation of State Key Laboratory of High-efficiency Utilization of Coal and Green Chemical Engineering (2022-K70), and the Hefei Advanced Computing Center for this work are gratefully acknowledged.

Data Availability Statement: Data generated or analyzed during this study are provided in full within the article.

Conflicts of Interest: The authors declare no conflict of interest.

References

1. Ooi, R.E.; Foo, D.C.; Ng, D.K.; Tan, R.R. Planning of carbon capture and storage with pinch analysis techniques. *Chem. Eng. Res. Des.* **2013**, *91*, 2721–2731. [CrossRef]
2. Hospital-Benito, D.; Lemus, J.; Moya, C.; Santiago, R.; Palomar, J. Process analysis overview of ionic liquids on CO_2 chemical capture. *Chem. Eng. J.* **2020**, *390*, 124509. [CrossRef]
3. Shi, Y.; Hou, S.; Qiu, X.; Zhao, B. MOFs-Based Catalysts Supported Chemical Conversion of CO_2. *Top. Curr. Chem.* **2020**, *378*, 11. [CrossRef] [PubMed]
4. Lan, J.; Qu, Y.; Zhang, X.; Ma, H.; Xu, P.; Sun, J. A novel water-stable MOF Zn(Py)(Atz) as heterogeneous catalyst for chemical conversion of CO_2 with various epoxides under mild conditions. *J. CO2 Util.* **2020**, *35*, 216–224. [CrossRef]
5. Singh, A.K.; Singh, S.; Kumar, A. Hydrogen energy future with formic acid: A renewable chemical hydrogen storage system. *Catal. Sci. Technol.* **2016**, *6*, 12–40. [CrossRef]
6. Aresta, M.; Dibenedetto, A.; Angelini, A. Catalysis for the Valorization of Exhaust Carbon: From CO_2 to Chemicals, Materials, and Fuels. Technological Use of CO_2. *Chem. Rev.* **2014**, *114*, 1709–1742. [CrossRef] [PubMed]
7. Leitner, W. Carbon-Dioxide as a Raw-Material—The Synthesis of Formic-Acid and Its Derivatives from CO_2. *Angew. Chem. -Int. Ed.* **1995**, *34*, 2207–2221. [CrossRef]
8. Kortlever, R.; Shen, J.; Schouten, K.J.P.; Calle-Vallejo, F.; Koper, M.T.M. Catalysts and Reaction Pathways for the Electrochemical Reduction of Carbon Dioxide. *J. Phys. Chem. Lett.* **2015**, *6*, 4073–4082. [CrossRef]
9. Hori, Y.; Wakebe, H.; Tsukamoto, T.; Koga, O. Electrocatalytic Process of Co Selectivity in Electrochemical Reduction of CO_2 at Metal-Electrodes in Aqueous-Media. *Electrochim. Acta* **1994**, *39*, 1833–1839. [CrossRef]
10. Whipple, D.T.; Kenis, P.J.A. Prospects of CO_2 Utilization via Direct Heterogeneous Electrochemical Reduction. *J. Phys. Chem. Lett.* **2010**, *1*, 3451–3458. [CrossRef]
11. Gao, D.; Zhou, H.; Cai, F.; Wang, J.-G.; Wang, G.; Bao, X. Pd-Containing Nanostructures for Electrochemical CO_2 Reduction Reaction. *Acs Catal.* **2018**, *8*, 1510–1519. [CrossRef]
12. Yoo, J.S.; Christensen, R.; Vegge, T.; Nørskov, J.K.; Studt, F. Theoretical Insight into the Trends that Guide the Electrochemical Reduction of Carbon Dioxide to Formic Acid. *Chemsuschem* **2016**, *9*, 358–363. [CrossRef] [PubMed]
13. Back, S.; Kim, H.; Jung, Y. Selective Heterogeneous CO_2 Electroreduction to Methanol. *Acs Catal.* **2015**, *5*, 965–971. [CrossRef]
14. Peterson, A.A.; Abild-Pedersen, F.; Studt, F.; Rossmeisl, J.; Nørskov, J.K. How copper catalyzes the electroreduction of carbon dioxide into hydrocarbon fuels. *Energy Environ. Sci.* **2010**, *3*, 1311–1315. [CrossRef]
15. Dinh, C.-T.; Burdyny, T.; Kibria, M.G.; Seifitokaldani, A.; Gabardo, C.M.; de Arquer, F.P.G.; Kiani, A.; Edwards, J.P.; De Luna, P.; Bushuyev, O.S.; et al. CO_2 electroreduction to ethylene via hydroxide-mediated copper catalysis at an abrupt interface. *Science* **2018**, *360*, 783–787. [CrossRef]

16. Gattrell, M.; Gupta, N.; Co, A. A review of the aqueous electrochemical reduction of CO_2 to hydrocarbons at copper. *J. Electroanal. Chem.* **2006**, *594*, 1–19. [CrossRef]
17. Nie, X.; Luo, W.; Janik, M.J.; Asthagiri, A. Reaction mechanisms of CO_2 electrochemical reduction on Cu(111) determined with density functional theory. *J. Catal.* **2014**, *312*, 108–122. [CrossRef]
18. Ren, D.; Fong, J.; Yeo, B.S. The effects of currents and potentials on the selectivities of copper toward carbon dioxide electroreduction. *Nat. Commun.* **2018**, *9*, 925. [CrossRef]
19. Reske, R.; Mistry, H.; Behafarid, F.; Cuenya, B.R.; Strasser, P. Particle Size Effects in the Catalytic Electroreduction of CO_2 on Cu Nanoparticles. *J. Am. Chem. Soc.* **2014**, *136*, 6978–6986. [CrossRef]
20. Choi, C.; Cheng, T.; Espinosa, M.F.; Fei, H.; Duan, X.; Goddard, W.A.; Huang, Y. A Highly Active Star Decahedron Cu Nanocatalyst for Hydrocarbon Production at Low Overpotentials. *Adv. Mater.* **2019**, *31*, e1805405. [CrossRef]
21. Ma, M.; Djanashvili, K.; Smith, W.A. Controllable Hydrocarbon Formation from the Electrochemical Reduction of CO_2 over Cu Nanowire Arrays. *Angew. Chem. Int. Ed.* **2016**, *55*, 6680–6684. [CrossRef] [PubMed]
22. Li, Y.; Cui, F.; Ross, M.B.; Kim, D.; Sun, Y.; Yang, P. Structure-Sensitive CO_2 Electroreduction to Hydrocarbons on Ultrathin 5-fold Twinned Copper Nanowires. *Nano Lett.* **2017**, *17*, 1312–1317. [CrossRef] [PubMed]
23. Feng, X.; Jiang, K.; Fan, S.; Kanan, M.W. A Direct Grain-Boundary-Activity Correlation for CO Electroreduction on Cu Nanoparticles. *ACS Cent. Sci.* **2016**, *2*, 169–174. [CrossRef] [PubMed]
24. Hirunsit, P.; Soodsawang, W.; Limtrakul, J. CO_2 Electrochemical Reduction to Methane and Methanol on Copper-Based Alloys: Theoretical Insight. *J. Phys. Chem. C* **2015**, *119*, 8238–8249. [CrossRef]
25. Zheng, X.; Ji, Y.; Tang, J.; Wang, J.; Liu, B.; Steinrück, H.-G.; Lim, K.; Li, Y.; Toney, M.F.; Chan, K.; et al. Theory-guided Sn/Cu alloying for efficient CO_2 electroreduction at low overpotentials. *Nat. Catal.* **2019**, *2*, 55–61. [CrossRef]
26. Kim, D.; Resasco, J.; Yu, Y.; Asiri, A.M.; Yang, P. Synergistic geometric and electronic effects for electrochemical reduction of carbon dioxide using gold-copper bimetallic nanoparticles. *Nat. Commun.* **2014**, *5*, 4948. [CrossRef] [PubMed]
27. Huang, J.; Mensi, M.; Oveisi, E.; Mantella, V.; Buonsanti, R. Structural Sensitivities in Bimetallic Catalysts for Electrochemical CO_2 Reduction Revealed by Ag-Cu Nanodimers. *J. Am. Chem. Soc.* **2019**, *141*, 2490–2499. [CrossRef]
28. Zhu, W.; Tackett, B.M.; Chen, J.G.; Jiao, F. Bimetallic Electrocatalysts for CO_2 Reduction. *Top. Curr. Chem.* **2018**, *376*, 41. [CrossRef]
29. Kim, D.; Xie, C.; Becknell, N.; Yu, Y.; Karamad, M.; Chan, K.; Crumlin, E.J.; Nørskov, J.K.; Yang, P. Electrochemical Activation of CO_2 through Atomic Ordering Transformations of AuCu Nanoparticles. *J. Am. Chem. Soc.* **2017**, *139*, 8329–8336. [CrossRef]
30. Zhang, S.; Kang, P.; Bakir, M.; Lapides, A.M.; Dares, C.J.; Meyer, T.J. Polymer-supported CuPd nanoalloy as a synergistic catalyst for electrocatalytic reduction of carbon dioxide to methane. *Proc. Natl. Acad. Sci. USA* **2015**, *112*, 15809–15814. [CrossRef]
31. Sarfraz, S.; Garcia-Esparza, A.T.; Jedidi, A.; Cavallo, L.; Takanabe, K. Cu-Sn Bimetallic Catalyst for Selective Aqueous Electroreduction of CO_2 to CO. *ACS Catal.* **2016**, *6*, 2842–2851. [CrossRef]
32. Choi, C.; Cai, J.; Lee, C.; Lee, H.M.; Xu, M.; Huang, Y. Intimate atomic Cu-Ag interfaces for high CO_2RR selectivity towards CH_4 at low over potential. *Nano Res.* **2021**, *14*, 3497–3501. [CrossRef]
33. Guan, W.; Zhu, H.; Zhang, Y.; Ren, X.; Ma, T.; Liu, A. Molecular structure design and interface behavior of ionic liquids on metal surfaces: A theoretical study. *Surf. Interfaces* **2022**, *34*, 102314. [CrossRef]
34. Liu, A.; Yang, Y.; Kong, D.; Ren, X.; Gao, M.; Liang, X.; Yang, Q.; Zhang, J.; Gao, L.; Ma, T. DFT study of the defective carbon materials with vacancy and heteroatom as catalyst for NRR. *Appl. Surf. Sci.* **2021**, *536*, 147851. [CrossRef]
35. Liu, A.; Guan, W.; Zhao, X.; Ren, X.; Liang, X.; Gao, L.; Li, Y.; Ma, T. Investigation on the interfacial behavior of polyorganic inhibitors on a metal surface by DFT study and MD simulation. *Appl. Surf. Sci.* **2021**, *541*, 148570. [CrossRef]
36. Liu, A.; Guan, W.; Wu, K.; Ren, X.; Gao, L.; Ma, T. Density functional theory study of nitrogen-doped graphene as a high-performance electrocatalyst for CO_2RR. *Appl. Surf. Sci.* **2021**, *540*, 148319. [CrossRef]
37. Liang, X.; Ren, X.; Guo, M.; Li, Y.; Xiong, W.; Guan, W.; Gao, L.; Liu, A. CO_2 electroreduction by AuCu bimetallic clusters: A first principles study. *Int. J. Energy Res.* **2021**, *45*, 18684–18694. [CrossRef]
38. Zhu, H.; Liang, Z.; Xue, S.; Ren, X.; Liang, X.; Xiong, W.; Gao, L.; Liu, A. DFT practice in MXene-based materials for electrocatalysis and energy storage: From basics to applications. *Ceram. Int.* **2022**, *48*, 27217–27239. [CrossRef]
39. Huang, X.; Tang, J.; Luo, B.; Knibbe, R.; Lin, T.; Hu, H.; Wang, L. Sandwich-Like Ultrathin TiS_2 Nanosheets Confined within N, S Codoped Porous Carbon as an Effective Polysulfide Promoter in Lithium-Sulfur Batteries. *Adv. Energy Mater.* **2019**, *9*, 1901872. [CrossRef]
40. Tang, Q.; Lee, Y.; Li, D.-Y.; Choi, W.; Liu, C.W.; Lee, D.; Jiang, D.-E. Lattice-Hydride Mechanism in Electrocatalytic CO_2 Reduction by Structurally Precise Copper-Hydride Nanoclusters. *J. Am. Chem. Soc.* **2017**, *139*, 9728–9736. [CrossRef]
41. Nie, X.; Jiang, X.; Wang, H.; Luo, W.; Janik, M.J.; Chen, Y.; Guo, X.; Song, C. Mechanistic Understanding of Alloy Effect and Water Promotion for Pd-Cu Bimetallic Catalysts in CO_2 Hydrogenation to Methanol. *ACS Catal.* **2018**, *8*, 4873–4892. [CrossRef]